www.czasopisma.pan.pl PAN POLSKA AKADEMIA NAUK www.journals.pan.pl

PAN ARCHIVES OF ACOUSTICS
Vol. **38**, No. 3, pp. 303–310 (2013)



*DOI: 10.2478/aoa-2013-0037*

# Discrimination of Acoustic Emission Signals for Damage Assessment in a Reinforced Concrete Slab Subjected to Seismic Simulations

Francisco A. SAGASTA, Juan L. TORNÉ, Antonio SÁNCHEZ-PAREJO, Antolino GALLEGO

*Department of Applied Physics, Building Engineering School, University of Granada*
18071 Granada, Spain; e-mail: antolino@ugr.es

(*received October 30, 2012; accepted February 7, 2013*)

The purpose of this work is to distinguish between Acoustic Emission (AE) signals coming from mechanical friction and AE signals coming from concrete cracking, recorded during fourteen seismic simulations conducted with the shaking table of the University of Granada on a reinforced concrete slab supported on four steel columns. To this end, a particular criterion is established based on the Root Mean Square of the AE waveforms calculated in two different temporal windows. This criterion includes a parameter calculated by optimizing the correlation between the mechanical energy dissipated by the specimen (calculated by means of measurements with accelerometers and displacement transducers) and the energy obtained from the AE signals recorded by low-frequency piezoelectric sensors located on the specimen. The final goal of this project, initiated four years ago, is to provide a reliable evaluation of the level of damage of Reinforced Concrete specimens by means of AE signals to be used in future Structural Health Monitoring strategies involving RC structures.

**Keywords:** acoustic emission, structural health monitoring, reinforced concrete structures, signal processing.

## 1. Introduction

Reinforced concrete (RC) structures located in earthquake-prone areas are susceptible to suffering damage caused by the cyclic loading induced by ground acceleration during seismic events. It is well known that moderate tremors, which may occur several times during the lifetime of a structure, produce damage of the concrete due to cracking.

Structural Health Monitoring (SHM) strategies and techniques can play an important role in this context in the future. The measurement, recording, and analysis of acoustic emission (AE) signals generated during a seismic event could prove very effective as a health monitoring technique when dealing with remote or inaccessible parts of a structure difficult to evaluate by means of other methods. To date, the AE technique has been applied to RC elements at the level of material (concrete) or individual elements (beams, columns) (Yuyama *et al.*, 1999; 2001), though little research has focused on assemblages of several structural elements (Carpinteri *et al.*, 2007); in the latter case, research involved the AE generated by relatively simple loadings such as vibrations induced by traffic. In this overall context, papers published by our research group in past years address damage assessment of RC structures subjected to low-cycle fatigue loads (Benavent-Climent *et al.*, 2009; 2010), and more recently, to complex dynamic loadings such as those induced by earthquakes (Benavent-Climent *et al.*, 2011; Gallego *et al.*, 2011). More information about the application of the AE technique to other fields can be found in (Guzik *et al.*, 2006; Wozniak *et al.*, 2006; Jasieński *et al.*, 2012).

However, the set of AE signals recorded during seismic events can be complicated, as it may be highly contaminated by sources of noise, mainly due to friction between different parts of the specimen or internal friction in the macrofractures and microfractures already opened inside the concrete. More details about internal cracks in concrete, including some interesting images in stereo optical and electron scanning microscopes, and the application of the AE technique for damage assessment, can be found in (Ranachowski *et al.*, 2012). For this reason, unveiling their relation with the damage accumulated on the structure requires considerable post-processing work on the set of AE signals recorded.

A simple procedure for discriminating between the AE signals coming from friction – *Type (ii)* – and those from concrete cracking – *Type (i)* – was already proposed in (Gallego, 2011). This algorithm is based on the definition of appropriate temporal windows in the AE waveforms, calculation of the RMS (Root Mean Square) in these windows, and establishment of a final comparison criterion of the RMS to decide if a particular AE signal is *Type (i)* or *Type (ii)*. Once the signals have been discriminated, the AE energy of the signals identified as *Type (i)*, from the concrete cracking, is calculated as a tentative index to evaluate the damage of the specimen (Gallego *et al.*, 2011).

In (Gallego *et al.*, 2011), a fixed criterion was put forth regarding the RMS in each window: a signal is *Type (i)* if the relationship $\mathrm{RMS}_1 \geq Q \cdot \mathrm{RMS}_2$ holds, $\mathrm{RMS}_1$ and $\mathrm{RMS}_2$ being the RMSs calculated in each temporal window. Some physical considerations were used to define the temporal width of the two windows, but not to acquire the criterion parameter $Q$. Moreover, the same $Q$ value was assumed for all the seismic events, even though this assumption obviously reduces the effectiveness of the signal discrimination procedure, because the level and number of friction AE signals – *Type (i)* – can be strongly dependent upon the severity of the seismic event.

This paper proposes a further improvement of the procedure described in (Gallego, 2011) by considering that parameter $Q$ depends on the severity of the seismic event. Namely, an algorithm is proposed to automatically estimate $Q$ in each seismic simulation; it is based on an optimization of the correlation between the mechanical energy dissipated by the specimen and the AE energy.

This optimized algorithm allows for a better classification of *Type (i)* and *Type (ii)* signals, and thus a closer correlation between mechanical and acoustic energies, providing a more accurate evaluation of the level of damage in the specimen.

Results of application with the optimized procedure are presented for a RC concrete slab supported on four steel columns subjected to seismic events of different severity, tested with the $3\times3$ m$^2$ MTS shaking table at the University of Granada.

## 2. Test model, experimental set-up, and instrumentation

A one-story (2.8 m height) and one-bay (4.8 m length) prototype structure consisting of a RC slab supported on four box-type steel columns was designed following current Spanish codes NCSE-02 (Ministry of Construction of Spain, 2002) and EHE-08 (Ministry of Construction of Spain, 2008). From the prototype structure, the corresponding test model was derived by applying the similarity laws described in (Benavent-Climent *et al.*, 2011). The depth of the slab was 125 mm. It was reinforced with steel meshes, one on the top made with 6 mm diameter bars spaced 100 mm, and another on the bottom consisting of 10 mm diameter bars spaced 75 mm. The average yield stress of the reinforcing steel was 467 MPa, and the average concrete strength was 23.5 MPa. The concrete was obtained by mixing together Portland cement, fine aggregate, coarse aggregate (maximum size 12.5 mm), superplasticizer additive CONPLAST SP-337, with the water-cement ratio 0.54. Concrete was vibrated for a few seconds and the specimen was cured at the room temperature of the laboratory for 28 days. The specimen was finally subjected to seismic loads after 15 additional days for its optimal instrumentation.

The model was tested with the uniaxial MTS $3\times3$ m$^2$ shaking table of the University of Granada (Spain) shown in Fig. 1. The bottom ends of the columns were fixed to the table by bolts. Similitude requirements between prototype and test model and the dead and live gravity loads were satisfied by attaching

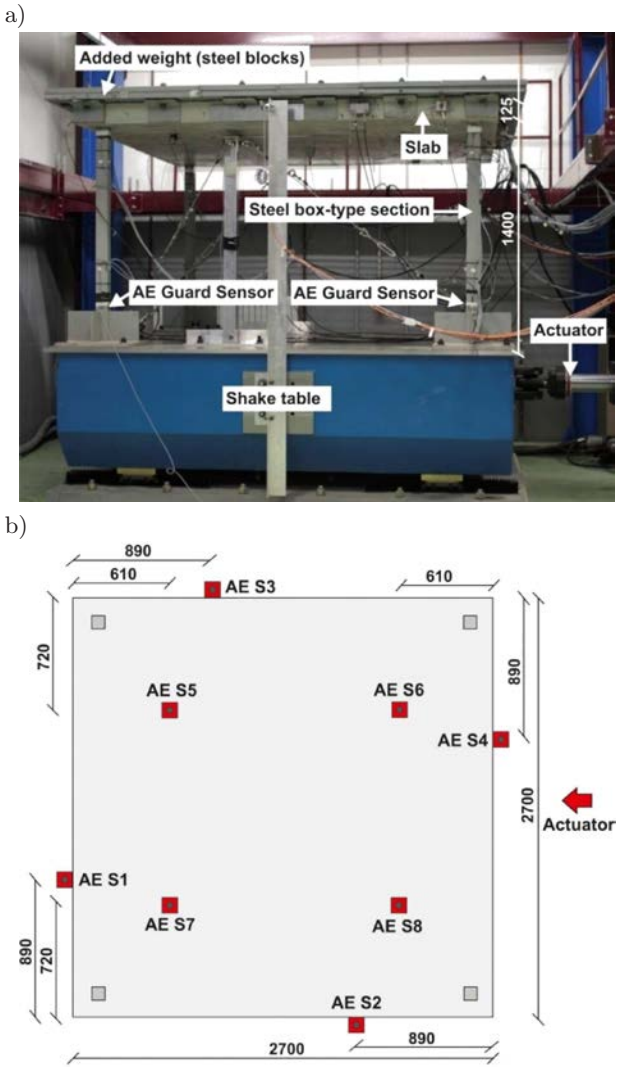


Fig. 1. Test model: a) elevation, b) plan.

additional steel blocks on the top of the RC slab. The total mass of the slab including the added steel blocks was $m = 7390$ kg. The acceleration record used for the shaking table tests reproduced the NS component of the 1980 Campano-Lucano earthquake recorded at Calitri (Italy). Two series of seismic simulations were applied to the test model. The same accelerogram was used in all simulations, the scaling factor of the peak accelerations (PA) being the only difference. The third column of Table 1 shows the PA applied in each simulation. The first series consisted of eight simulations with PA increasing progressively from $0.08g$ to $0.58g$ (where $g$ is the acceleration of gravity). The second series consisted of six simulations with PA increasing from $0.19g$ to $0.95g$, this series starting with values of PA smaller than the maximum obtained in the first series. That is, in several simulations of the second series, the test model was subjected to load levels smaller than the ones previously undergone, so that the simulations reproduced two types of situations on the structure: (i) the AE energy and plastic strain energy were dominated by the new damage associated with the opening and extension of cracks; and (ii) the AE energy and hysteretic energy were dominated by friction generated from the existing damage. Both situations are realistic scenarios that a structure may experience over its lifetime.

Table 1. Seismic Simulations (name and Peak Acceleration (PA)).

| Test series | | PA ($g$) |
|---|---|---|
| 1 | 2 | |
| Simulation (in order of application) | | |
| A1 | | 0.08 |
| B1 | | 0.10 |
| C1 | | 0.12 |
| D1 | | 0.19 |
| E1 | | 0.29 |
| F1 | | 0.38 |
| G1 | | 0.44 |
| H1 | | 0.58 |
| | A2 | 0.19 |
| | B2 | 0.38 |
| | C2 | 0.58 |
| | D2 | 0.66 |
| | E2 | 0.74 |
| | F2 | 0.95 |

Displacements, strains, and accelerations were acquired simultaneously during each seismic simulation. The relative horizontal displacement between the shaking table and the slab was measured by LVDT (Linear Variable Differential Transformer) displacement transducers. Accelerometers were fixed to the shaking table and to the slab, to measure the absolute acceleration of the table and the absolute response acceleration of the slab in the direction of shaking, respectively. The parameter called the mechanical energy dissipated by concrete was obtained for all data. See (Benavent-Climent *et al.*, 2011) for details.

A Vallen System ASMY-5 was used to measure the AE signals during testing. Eight VS30 AE flat low-frequency sensors were placed on the specimen at the eight positions indicated in Fig. 1. These sensors were set in the range 20–80 kHz, using the 25–180 kHz frequency band during signal acquisition with a sample period of 1.6 μs and 1024 data for recording waveforms (200 of them, before the arrival time). Thus, the entire duration of the record window was $t_{\max} = 1318$ μs.

Before testing, the electric noise in the laboratory was measured and a calibration test was carried out by breaking pencil leads (Hsu-Nielsen source) along the specimen. Thus, it was established that using 45 dB as the threshold of detection, pencil leads broken at any place on the specimen could be recorded by all the sensors. Moreover, in an attempt to prevent or reduce friction noise generated between the different metallic elements located in the specimen (added steel blocks, screws, fixing systems of sensors, accelerometers, LVDTs, etc.), rubbers and teflon films were inserted between any two contacting surfaces susceptible of generating noise.

## 3. AE signal discrimination procedure

Firstly, detailed observation of the AE waveforms recorded in all sensors was made. From it, two patterns of signals were found to be qualitatively different:

*Type (i)*: short-duration signals, whose energy was concentrated mainly at the beginning of the signal, and whose duration was not excessively great;

*Type (ii)*: long-duration signals, whose energy was not concentrated at the beginning of the signal but distributed along the whole signal.

It was observed that both types of signals had largely varying durations and amplitudes, a feature that complicates their separation by traditional filters based only on the classic parameters of AE signals (amplitude, duration, rise-time, etc.). Therefore, developing a post-processing means of identifying and discriminating these signals was mandatory.

The discrimination procedure departs from the premise, based on bibliographical documentation and our own experience with this type of material, that the short-duration signals referred to above as *Type (i)* can correspond to concrete cracking, whereas the long-duration signals designated as *Type (ii)* can be statistically associated with various spurious sources (mainly friction).

As the *first step* of the discrimination process, the following temporal windows were defined in all the AE waveforms (see Fig. 2):

$W_1$ **(window 1):** 0–450 μs. Samples from $N = 0$ to $N = N_1$, with $N_1 = 281$;

$W_2$ **(window 2):** 450–1300 μs. Samples from $N = N_1 + 1$ to $N = N_2$, with $N_2 = 824$.

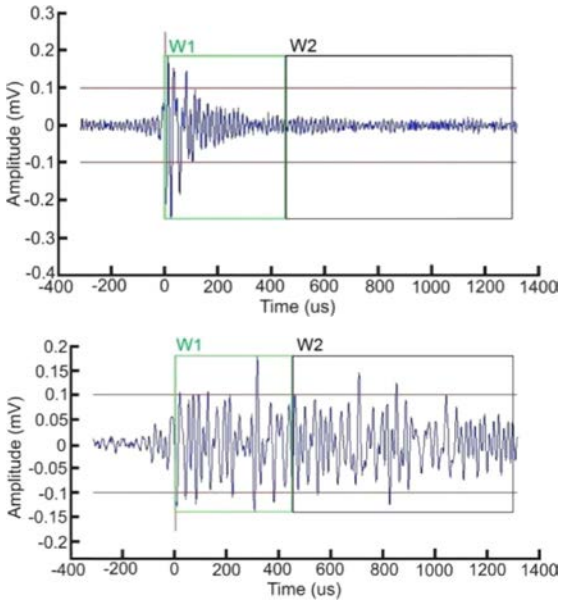


Fig. 2. Some AE Signals corresponding to simulation D1. Top: *Type (i)*; Bottom: *Type (ii)*. Windows $W_1$ and $W_2$ are marked on the signals.

The length of $W_1$ was established in view of the following physical criteria. The propagation speed of longitudinal waves in a bar of this kind of concrete was measured, yielding 3200 m/s. Thus, as the maximum distance between the center of the structure and the sensors was 1.44 m, the maximum arrival time was 450 μs, the time used for $W_1$. The second window duration ($W_2$) was from the end point $W_1$ (450 μs) to the end of the wave (1300 μs).

As the *second step*, the RMS in both windows was calculated. It is defined as

$$\mathrm{RMS}_1 = \sqrt{\frac{1}{N_1}\sum_{N=0}^{N_1} x_i^2}, \tag{1}$$

$$\mathrm{RMS}_2 = \sqrt{\frac{1}{N_2 - N_1}\sum_{N=N_1+1}^{N_2} x_i^2}, \tag{2}$$

where $x_i$ is the discretized AE signal.

As the *third step*, the following criterion was established to discriminate between *Type (i)* and *Type (ii)* signals:

$$\text{If } \mathrm{RMS}_1 \geq Q \cdot \mathrm{RMS}_2 \rightarrow \textit{Type } (i), \tag{3}$$

$$\text{If } \mathrm{RMS}_1 < Q \cdot \mathrm{RMS}_2 \rightarrow \textit{Type } (ii), \tag{4}$$

where the parameter $Q$ needs to be previously determined as explained in the Section below.

## 4. Optimization procedure for obtaining parameter $Q$

A range of values of $Q$ was previously set to carry out the search during the optimization process. Thus, for each particular value $Q_i \in [Q_1,\ Q_2]$, two physical variables were calculated:

- The acoustic energy MARSE (Measured Area under Rectified Signal Envelope) for all the AE waveforms meeting the condition given in Eq. (3), i.e. for signals of *Type (i)*. The accumulated value of this energy over a particular seismic event, normalized by its value at the end of this seismic event, was calculated for each value of $Q_i$. It was denoted $E_i^{\mathrm{AE}}(t)$, where $t$ is the time along the seismic event normalized to its maximum value (this normalized time named pseudotime, from $t = 0$ to $t = 1$). Note that $E_i^{\mathrm{AE}}(t)$ depends strongly on the value of $Q_i$, because it is calculated only for *Type (i)* signals, and the set of these signals depends on the criterion used for discriminating (Eqs. (3) and (4)).
- The mechanical energy dissipated by the specimen in the course of the seismic event, $W_p(t)$, normalized by its value at the end the seismic event (see (Benavent-Climent, 2011) for details to calculate this energy). Obviously, this energy is totally independent on the value of $Q_i$, because it is not based on acoustic emission measurements.

After calculating both energies, the following quantity was calculated in order to make a comparison and minimize the differences between them:

$$D_{Q_i} = \sqrt{\int_0^1 \left|(E_i^{\mathrm{AE}})^2 - (W_p^2)\right| \,\mathrm{d}t}. \tag{5}$$

Finally, the optimum value of $Q$, denoted $O_{\mathrm{opt}}$, was established as the one that locally minimizes $D$ defined in Eq. (5) in the range of values $Q_i \in [Q_1,\ Q_2]$, i.e.

$$Q_{\mathrm{opt}} = \min_{Q_i \in [Q_1, Q_2]} \{D_{Q_i}\}. \tag{6}$$

## 5. Results

The optimization procedure to discriminate the signals was applied to the fourteen seismic simulations conducted with a shaking table, using the range of values $Q_i \in [Q_1,\ Q_2] = [0.6,\ 2]$, beyond which the results proved to be inconsistent. A step of 0.05 was used for $Q_i$ in this range. Table 2 shows the optimum value obtained for $Q$ in all the seismic events, while Fig. 4 shows a superimposed comparison of the accumulated mechanical and acoustic energies, $W_p(t)$ and $E_i^{AE}(t)$,

Table 2. $Q_{opt}$ values obtained for each seismic simulation.

| Test | PA ($g$) | $Q_{opt}$ |
|---|---|---|
| A1 | 0.08 | 1.68 |
| B1 | 0.10 | 1.23 |
| C1 | 0.12 | 1.06 |
| D1 | 0.19 | 1.94 |
| E1 | 0.29 | 0.60 |
| F1 | 0.38 | 0.60 |
| G1 | 0.44 | 0.60 |
| H1 | 0.58 | 0.60 |
| A2 | 0.19 | 1.53 |
| B2 | 0.38 | 1.08 |
| C2 | 0.58 | 1.44 |
| D2 | 0.66 | 1.99 |
| E2 | 0.74 | 1.68 |
| F2 | 0.95 | 1.99 |

in all the seismic events. It can be clearly seen that, in general and as intended, there is a reasonably good correlation between them, indicating the effectiveness of the discrimination algorithm proposed. Moreover, comparison of these correlations and those previously published in (Gallego, 2011) reveals a clear improvement, supporting the optimization procedure proposed here.

As an example, Fig. 3 shows 6 signals classified as *Type (i)* (three on the left side) and *Type (ii)* (three on the right side), respectively. Simple visual inspection confirms that all were correctly classified.

Finally, Fig. 5 plots both the acoustic energy and the mechanical energy dissipated by the specimen, accumulated over all the seismic events. Both energies are normalized to their values at the end of event F1, the point at which plastification of the steel began to occur (as corroborated by strain gages attached on the steel in the columns and the reinforcements (Benavent-Climent, 2011)). It is evident that

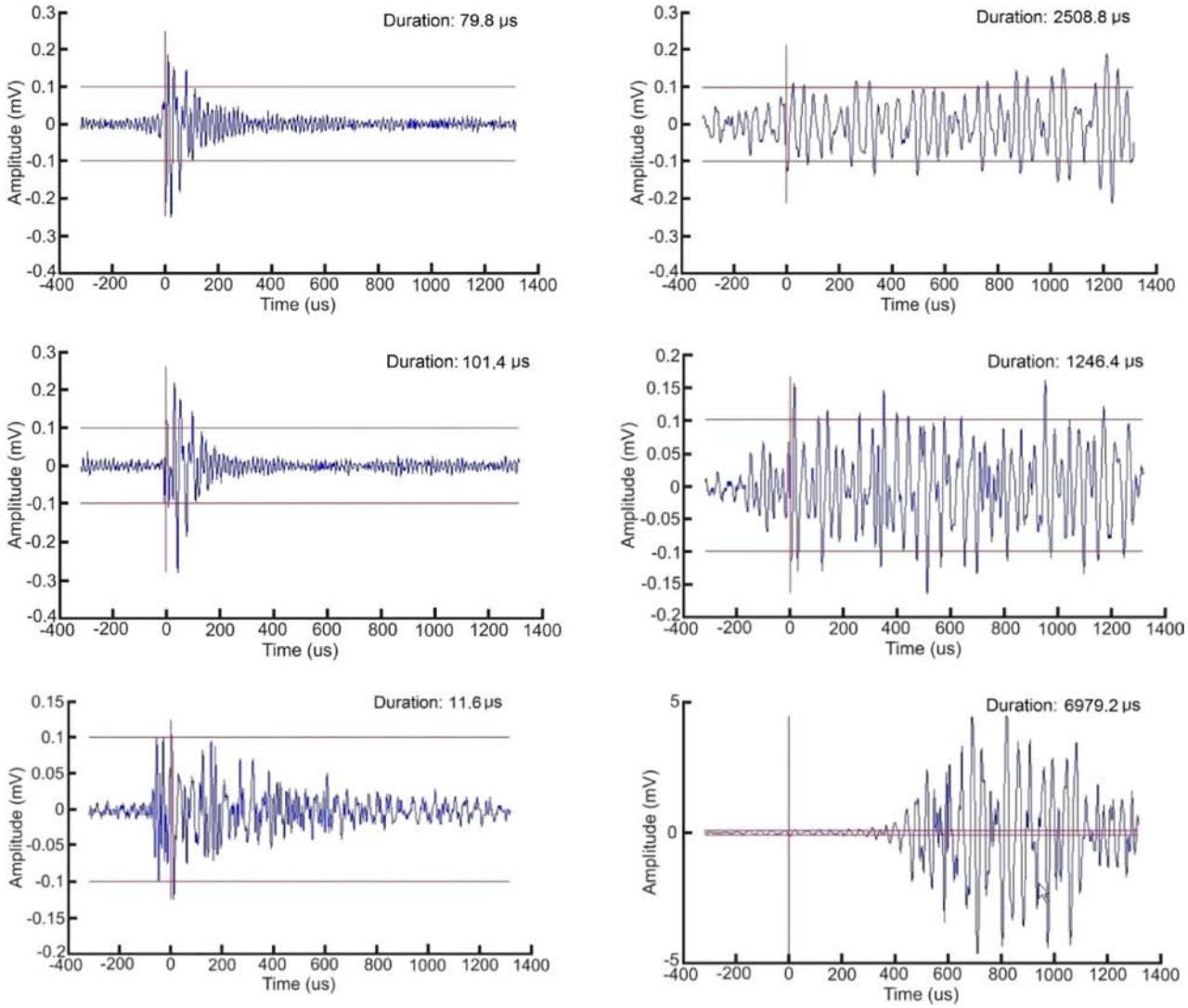


Fig. 3. Some AE Signals corresponding to simulation D1. Left column: *Type* ($i$); Right column: *Type (ii)*.

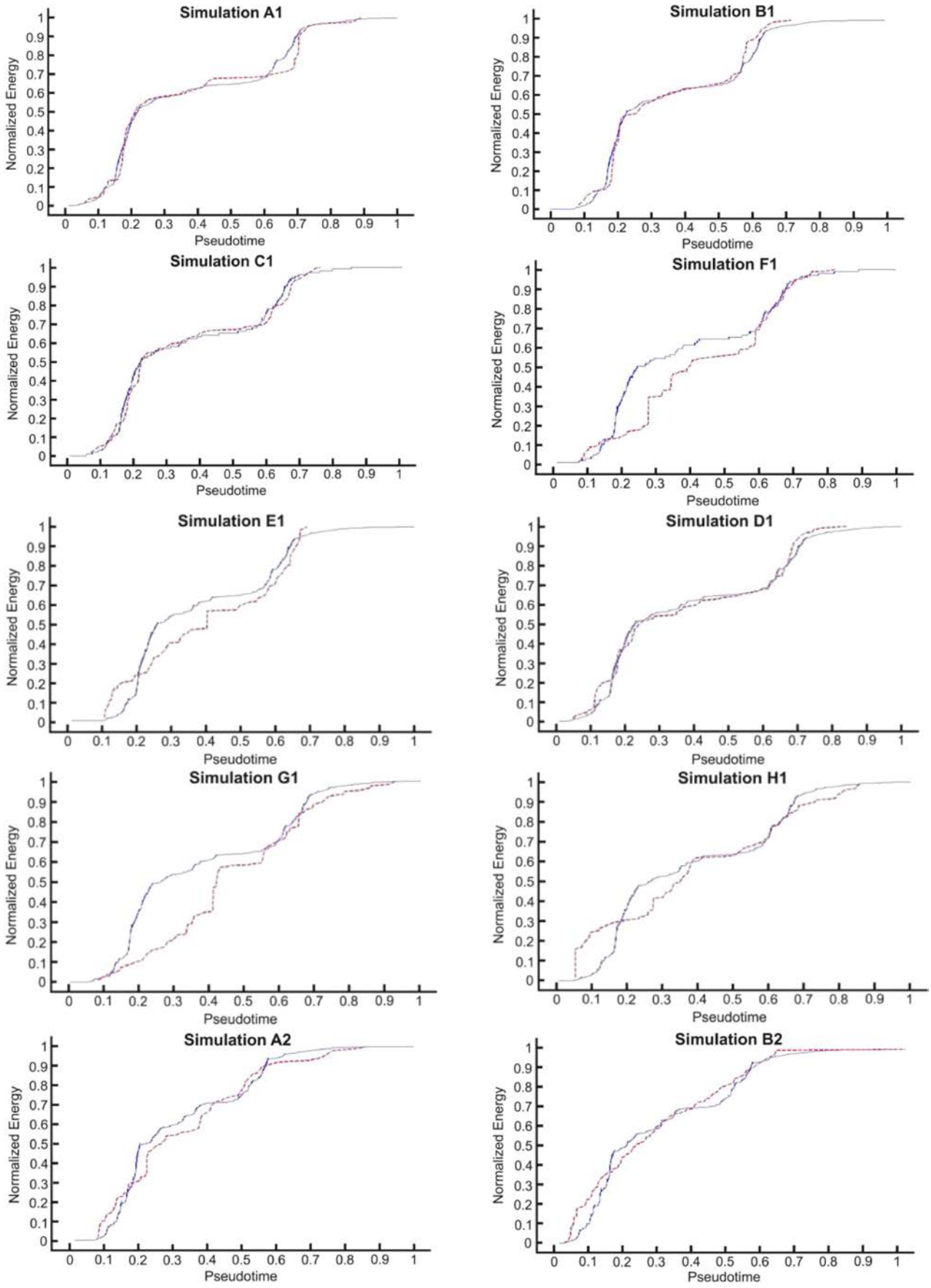
Simulation A1
Simulation B1
Simulation C1
Simulation F1
Simulation E1
Simulation D1
Simulation G1
Simulation H1
Simulation A2
Simulation B2
Normalized Energy
Pseudotime

[Fig. 4]

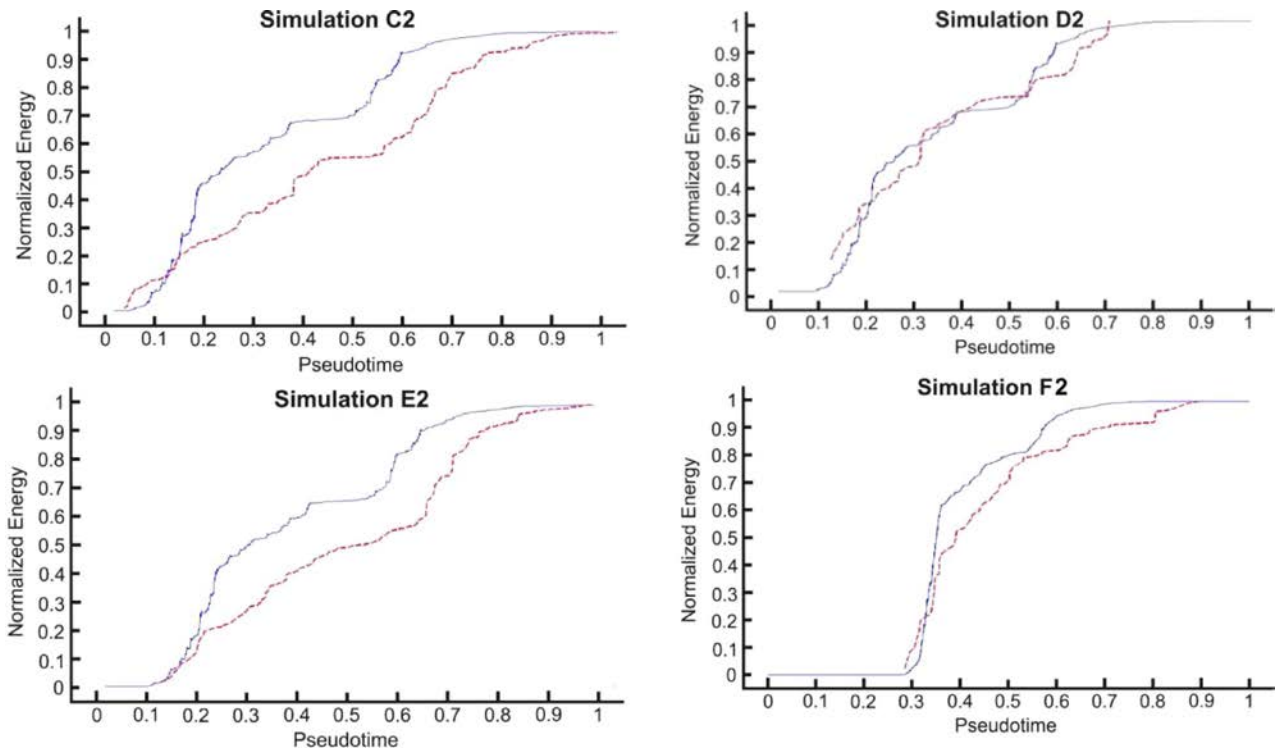


Fig. 4. Normalized $E^{AE}$ (red dotted line) and $W_p$ (blue solid line) for each seismic simulation.

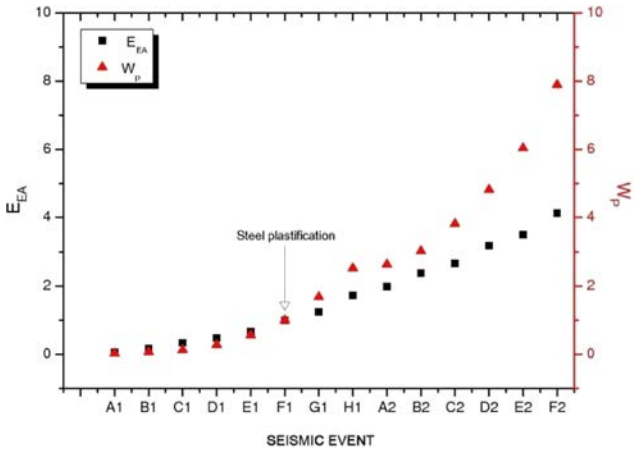


Fig. 5. $W_p$ and $E^{AE}$ energies accumulated along the whole load history, normalized by their respective values at the end of simulation F1.

before this point (F1), there is an excellent correlation between the two energies, thus demonstrating that the AE energy is an adequate indicator for cracking level evaluation in the RC structure. However, from this point on, there is a clear separation between the two energies (always $E^{AE} < W_p$) because the AE produced by the plastification of the steel cannot be recorded with the AE instrumentation used and the high threshold set for detection (45 dB). It is very well known that steel plastification usually produces AE amplitudes lower than 30 dB. For this reason, it is physically justified that when steel plastification occurs, the $E^{AE}$ remains consistently lower than $W_p$ (see (Benavent-Climent, 2011) for details).

## 6. Conclusions

An improvement of the algorithm proposed in (Gallego, 2011) to discriminate AE signals mainly coming from friction and signals from concrete cracking was presented. It was improved by introducing an optimization process for the difference between the AE energy and the mechanical energy dissipated by the specimen. The proposal provides a better match between these two energies and for all the seismic events carried out on the test specimen. The plastic strain energy $W_p$ is commonly accepted as an appropriate parameter for characterizing low-cycle fatigue damage in RC components, and it is used in well-established RC damage indexes. The finding that there is a good correlation between $W_p$ and AE energy, calculated by means of AE signals filtered through the procedure proposed, suggests that AE energy can be used as a parameter to quantitatively assess the level of damage in an RC structure subjected to seismic loading. Ongoing research aims to develop new damage indexes for RC structures subjected to seismic loadings expressed merely in terms of AE energy.

## Acknowledgments

This research received the financial support of the local government of Spain, Consejería de Innovación,

Ciencia y Tecnología, Project P07-TEP-02610. The work also received support from the European Union (Fonds Européen de Dévelopment Régional) and the Scholarship of Initiation to the Investigation of the University of Granada Research Plan (Beca de Iniciación a la Investigación del Plan Propio de la Universidad de Granada). The authors thank Prof. Benavent-Climent for his scientific contributions.

## References

1. Benavent-Climent A., Castro E., Gallego A. (2009), *AE Monitoring for Damage Assessment of RC Exterior Beam-Column Subassemblages Subjected to Cyclic Loading*, Structural Health Monitoring, **8**, 175–189.
2. Benavent-Climent A., Castro E., Gallego A. (2010), *Evaluation of low cycle fatigue damage in RC exterior beam-column subassemblages by acoustic emission*, Construction and Building Materials, **24**, 1830–1842.
3. Benavent-Climent A., Gallego A., Vico J.M. (2011), *An acoustic emission energy index for damage evaluation of reinforced concrete slabs under seismic loads*, Structural Health Monitoring, **11**, 1, 69–81.
4. Carpinteri A., Lacidogna G., Pugno N. (2007), *Structural damage diagnosis and life-time assessment by acoustic emission monitoring*, *Engineering Fracture* Mechanics, **74**, 1–2, 273–289.
5. Gallego A., Benavent-Climent A., Cristóbal I. (2011), *Health monitoring of reinforced concrete slabs subjected to earthquake-type dynamic loading via measurement and analysis of acoustic emission signals*, Smart Structures and Systems, **8**, 4, 385–398.
6. Guzik J., Wojtyniak M., Olszowski S., Marczak M., Ranachowski Z. (2006), *Investigation of acoustic emission signal generated in the friction pair lubricated with oils containing various lubricity additives*, Engineering Transactions, **54**, 2, 159–166.
7. Jasieński Z., Pawelek A., Piatkowski A., Ranachowski Z. (2009), *Twinning and shear band formation in channel-die compressed silver single crystals identified by Acoustic Emission method*, Archives of Metallurgy and Materials, **54**, 1, 29–33.
8. Ministry of Construction of Spain (2002), *Spanish Seismic Code NCSE-02*, Madrid.
9. Ministry of Construction of Spain (2008), *Spanish Concrete Code EHE-08*, Madrid.
10. Ranachowski Z., Jóźwiak-Niedźwiecka D., Brandt A.M., Dębowski T. (2012), *Application of the acoustic emission technique to determine critical stress in fiber reinforced mortar beams*, Archives of Acoustics, **37**, 3, 261–268.
11. Wozniak T.Z., Ranachowski Z. (2006), *Acoustic Emission during austenite decomposition into lower bainite with midrib*, Archives of Acoustics, **31**, 3, 319–334.
12. Yuyama S., Li ZW., Ito Y., Arazoe M. (1999), *Quantitative analysis of fracture process in RC column foundation by moment tensor analysis of acoustic emission*, Construction and Building Materials, **13**, 1–2, 87–97.
13. Yuyama S., Li ZW., Yoshizawa M., Tomokiyo T., Uomoto T. (2001), *Evaluation of fatigue damage in reinforced concrete slab by acoustic emission*, NDT&E International, **34**, 6, 381–387.